K. Andresen, R. Ritter* and E. Steck**

Theoretical and Experimental Investigations of Fracture by FEM and Grating Methods

REFERENCE Andresen, K., Ritter, R. and Steck, E., **Theoretical and experimental investigations of fracture by FEM and grating methods**, *Defect Assessment in Components – Fundamentals and Applications*, ESIS/EGF9 (Edited by J. G. Blauel and K.-H. Schwalbe) 1991, Mechanical Engineering Publications, London, pp. 345–361.

ABSTRACT A finite element technique allowing crack extension in arbitrary directions in elastic–plastic bodies is outlined, and grating methods with image processing for accompanying experimental investigations are presented. Using an extension of the Griffith crack growth criterion for elastic–plastic material, crack extension behaviour of inhomogeneously weld-simulated specimens was investigated numerically. Good agreement between experiment and numerical simulation was found, giving some insight into the energy flow near the crack tip of an inhomogeneous elastic–plastic material.

Numerical simulation of crack extension

Numerical simulation of crack growth in elastic–plastic bodies is usually done by analysing a symmetric specimen under symmetric loading. In this case only half of the body has to be modelled, and the plane containing the crack can be located on the boundary of the model. The basic idea of the most widely used crack growth techniques is to replace the boundary conditions by the reaction forces and then to release these forces in several steps **(1)(2)**.

This procedure can be readily adopted for non-symmetric problems. However, an automatic re-meshing algorithm has to be implemented to allow crack extension in an arbitrary direction. Details are given in **(3)**.

To calculate the energy release rate, it was necessary to allow finite crack steps in arbitrary directions. A special control strategy allowing testwise opening of all FE-edges adjacent to the crack tip was implemented into the FE-program. The crack extension path which led to the maximum energy release rate could then be chosen for further calculations.

Energy flow

Loading a body by forces $\boldsymbol{F}_i$, or by displacements $\boldsymbol{u}_i$, stresses $\boldsymbol{\sigma}_{kl}$, and strains ε_{kl} are induced. They give the specific work

$$W_s = \int_0^{\varepsilon} \sigma_{ij}\, d\varepsilon_{ij} \tag{1}$$

* Mechanik-Zentrum, Technische Universität Braunschweig, D-3300 Braunschweig, FRG.

Integrating over the volume of the body, the strain energy

$$W_{ges} = \int_V W_s \, dV \tag{2}$$

can be calculated. If a crack is extended at given forces or displacements, three energy consuming or energy producing processes have to be considered.

(1) If the body is loaded by forces F_i the points where the forces act will be displaced by $d\boldsymbol{u}_i$. The released energy is

$$dW_{load} = \boldsymbol{F}_i \cdot d\boldsymbol{u}_i \tag{3}$$

If the body is loaded by given displacements this expression vanishes.

(2) Changes in stresses and strains will cause some change dW_{el} of the elastically stored energy. (Notation: If energy is elastically stored, dW_{el} is positive).

(3) When forming the new surface or shifting the plastic zone, some energy dW_{diss} will be dissipated. In applications considered in this paper, energy dissipation by plastic deformation largely exceeds all other effects. They will therefore be neglected.

The amount of energy available to extend the crack is given by

$$dW_{rel} = dW_{load} - (dW_{el} + dW_{diss}) \tag{4}$$

Dividing by the crack length da, we arrive at the energy release rate

$$G = \frac{dW_{rel}}{da} \approx \frac{\delta W_{rel}}{\delta a} \tag{5}$$

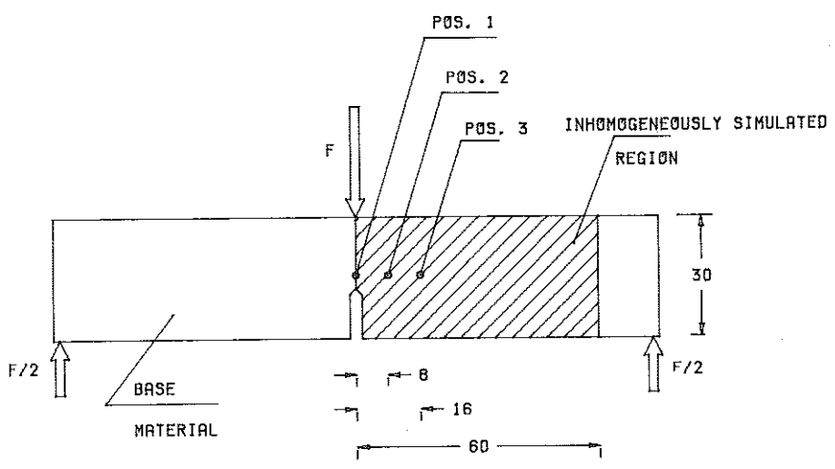

Fig 1 SEN specimen with inhomogeneously weld-simulated area

Fracture criterion

Based on equation (5) a fracture criterion can be given readily.
Crack extension will occur as soon as the energy release rate G reaches a critical value G_c

$$G = G_c \tag{6}$$

The direction of crack extension is given by that direction where G has its maximum.

While the well-known Griffith fracture criterion was formulated for elastic bodies **(4)**, this is a generalisation for elastic–plastic material.

Numerical investigations of weld-simulated specimens

In order to permit a comparison of experimental and numerical results a series of SEN specimens (150 × 30 × 15 mm^3), machined from 20 MnMoNi 5 5 steel with large, inhomogeneously weld-simulated regions was tested, Fig. 1. Micro-samples with a diameter of 3 mm were taken from the base material and from the inhomogeneously weld-simulated regions at different positions to give the stress–strain relations (Fig. 2). Figure 3 shows the finite element mesh related to the specimens. The plastic zone at the beginning of stable crack growth can be seen from Fig. 4. It was well represented by the finite element results when plane stress conditions were assumed.

Figures 5(a) and 5(b) show results of energy flow calculations for a constant value of crack extension assuming plane stress and plane strain conditions.

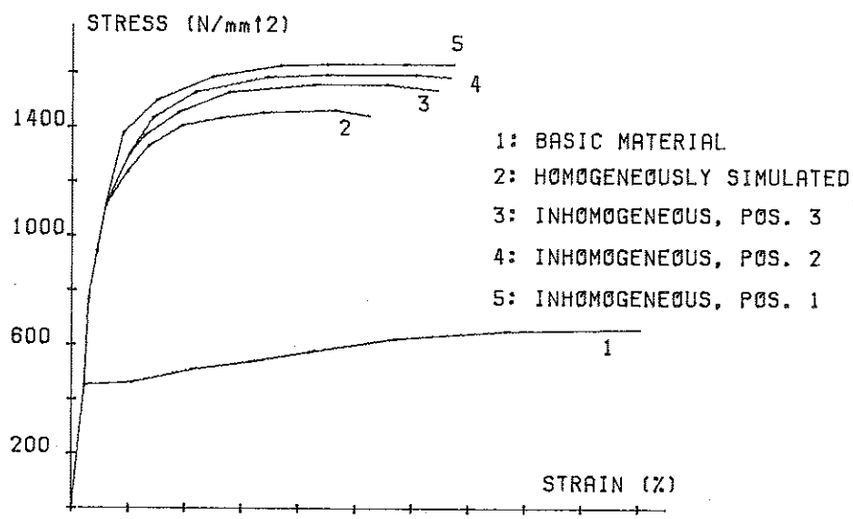

Fig 2 Stress–strain relations of different weld-simulated samples

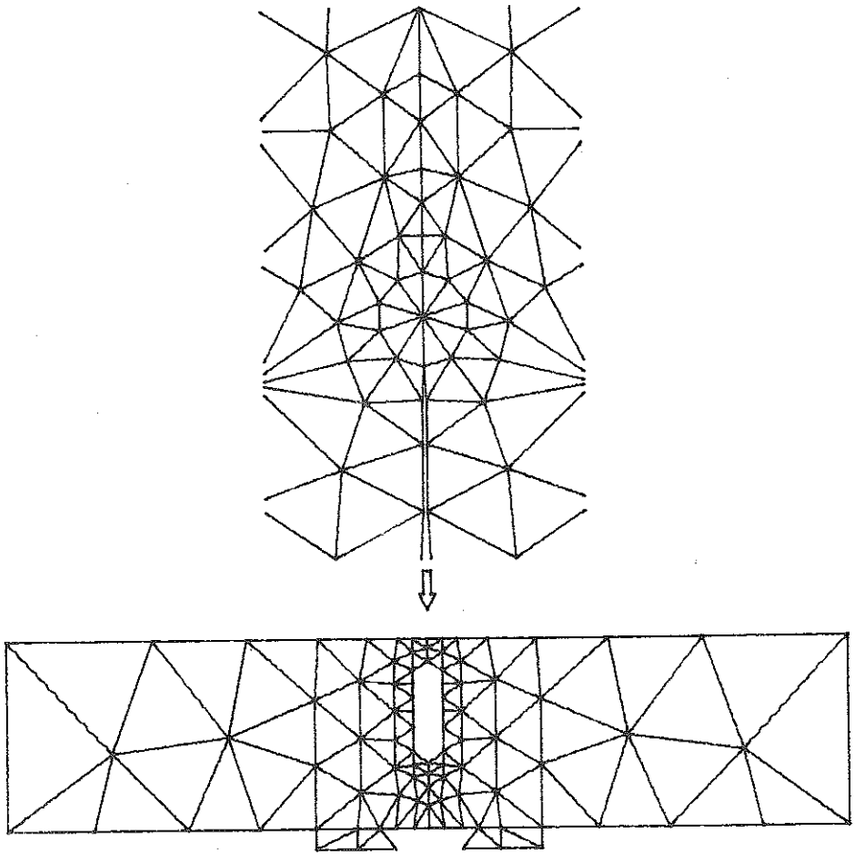

Fig 3 Finite element mesh

The abbreviations at the sides of the diagrams have the same meaning as in the section on energy flow. As the experiments were displacement controlled, the released energy dW_{rel} equals dW_{ges}.

During quasi-static loading of the specimen, stable crack extension occurs, and some deviation of the crack extension direction from the original crack plane has to be expected. Figure 4 shows the plastic zone of a pre-cracked inhomogeneously weld-simulated 20 MnMoNi 5 5 steel. Surprisingly the crack propagates in that region where the extension of the plastic zone is large and where more energy is dissipated compared to crack extension in other directions.

Examining the diagrams, the effect of crack deviation into the area of a larger plastic zone can be explained. As could be expected the upper curve representing the dissipated energy has its maximum at an angle of deviation of about 30 degrees. However, due to the large amount of elastic energy stored in

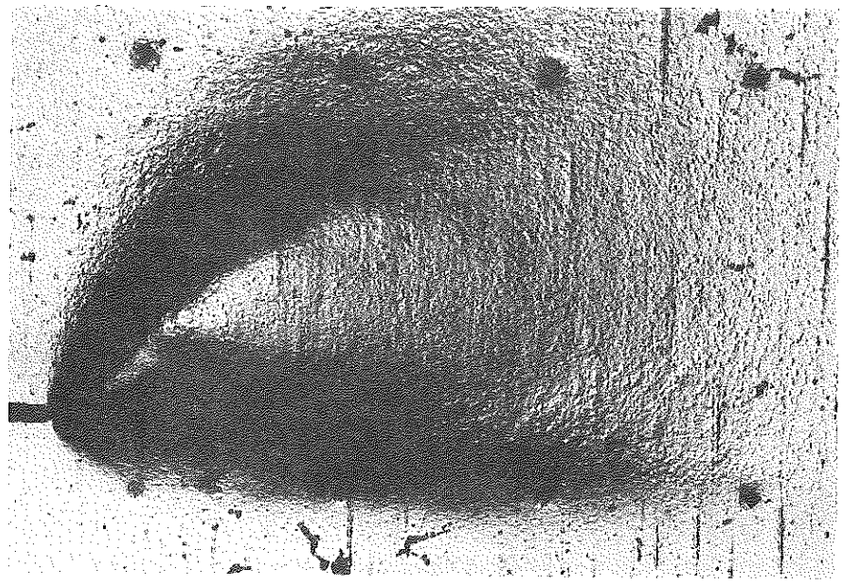

Fig 4 Plastic zone of inhomogeneously weld-simulated specimen

the plastic zone the maximum of the energy released by elastic unloading lies at about 30 degrees, too. In the case of plane stress the angle of deviation of the maximum energy release rate, which was calculated by interpolation, was found to be 19.4 degrees. This is in good agreement with the experimental result of about 25 degrees at the surface of the specimen.

Under plane strain conditions, which govern the deformation state in the centre of a thick walled specimen, no significant deviation of the crack is predicted (Fig. 5b). Looking at these results from a more general point of view, it has to be stated that the material properties at some distance of the crack tip have a significant influence on the fracture behaviour.

For a more detailed examination of crack behaviour and strain- and stress-fields in cracked specimens, experimental methods are under development, which allow by the use of *grating methods* and *image processing* the measurement of these magnitudes over extended areas of the specimen.

Grating methods

Principle

The grating methods are based on optical marks, which are combined in a given manner to the considered object surface (**5**). The relationship between object, marks, and their image leads to the geometrical properties of its surface.

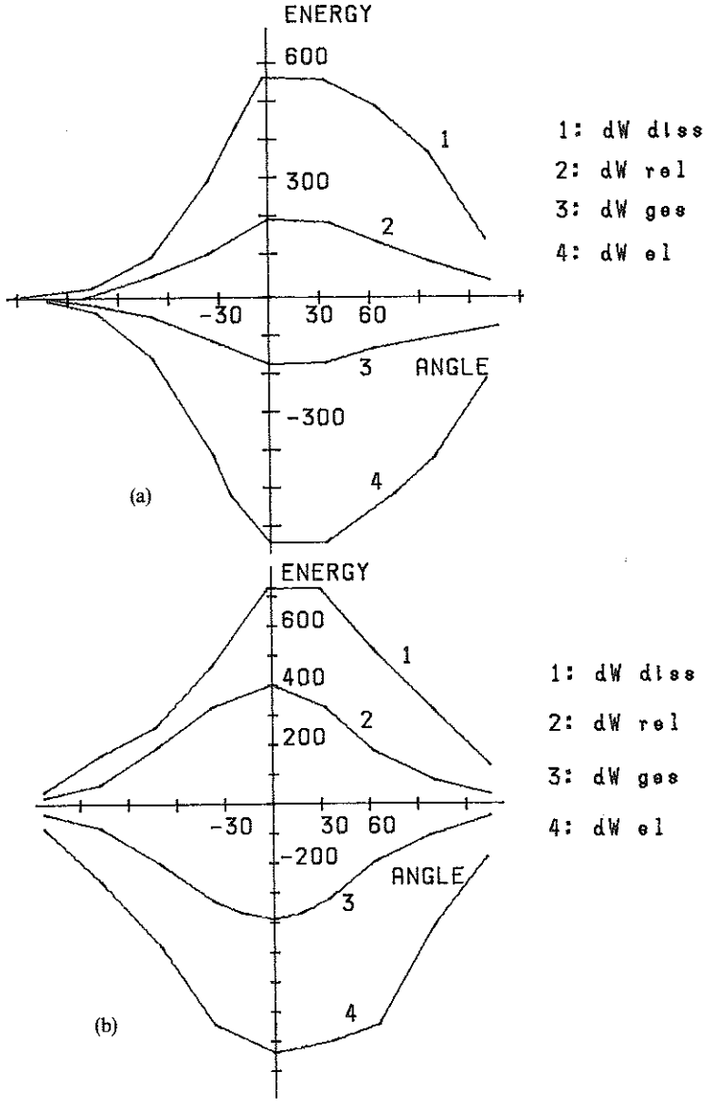

Fig 5 Energy flow, (a) plane stress, (b) plane strain

In this case, the optical marks are used for describing coordinates by their intensity profile, Fig. 6.

For experimental analysis of problems of fracture mechanics such marks are attached to the surface of the specimen, characterising the position of the related object points. Recording the marks by the stereophotographic principle, their global coordinates can be determined.

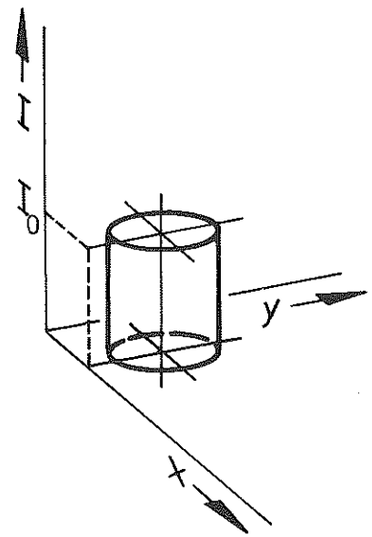

Fig 6 Optical mark, characterised by the intensity distribution $I(x, y)$ of a circular area ($I = I_0$) on a background ($I = 0$)

A pattern consisting of several marks is called a grating. For example, the centres of the spots of a point grating lead to the contour of the related object surface, whereby the completeness of its description depends on the density of the grating. The object and the grating are deformed in the same manner if the object is loaded.

Relating the difference of the change of position of two neighbouring marks of the grating to their distance, one obtains the average strain of the field, which is limited by these two marks.

Grating

A suitable procedure for producing gratings which are applicable also for high temperatures consists in spraying an emulsion of photoresist and titandioxid on the polished surface of the specimen, and to expose it through a mask **(6)**. After developing the exposed coating, the desired grating structure is available. By this method line densities up to 500 l/mm (lines per millimetre) were achieved without difficulties. Figure 7 shows a cross-grating with 5 l/mm at room temperature and at 850°C after a loading time of 30 minutes. In order to avoid the forming of tinder, the specimen was immersed in nitrogen. At temperatures above 180°C the photoresist evaporates and only the titandioxid can be observed. Using small grains of titandioxid with a diameter of 0.2–0.3 μm, sharp-edged grating lines are obtained. Due to the deformation of the object, cracks in the grating arise without a local detaching of the grating from the surface of the specimen.

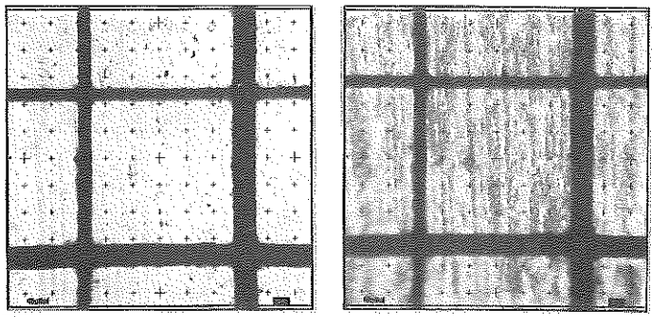

(a) (b)

Fig 7 Combined photoresist–titandioxid grating with 5 l/mm in a bright field observation, (a) room temperature, (b) 850°C

Experiment

Deformation and strain were measured at a plane specimen with a notch loaded in bending (7), Fig. 1. The whole-field measurement was performed over a range around the tip of a crack, which, growing from the tip of the notch, extended vertically towards the longitudinal axis of the specimen with increasing load.

Registration

The grating structure was recorded with a camera (Rollei 6006 Reseau) for different steps of loading or deformation, respectively. For facilitation of the digital picture processing, a uniform illumination of the test field is desirable. It can be achieved by sending light through a circular slit aperture which is connected to the front of the camera objective. This kind of lighting is suitable especially for the case of plane fields. To avoid disturbing influences from the environment, e.g. vibrations from a testing equipment during the recording, it is practical to use an electronic flash coupled with the aperture. Figure 8 shows a grating structure covering the field around the crack. For this case only the plane deformation was considered.

Image processing

As the strain is derived from second differences of the coordinates, as mentioned, and these are very sensitive to even small errors, the calculation of these coordinates from the images of the deformed grating requires high accuracy of the related image processing methods. A direct recording by a digital CCD camera is possible only if the area of interest is small and does not move during the different stages of deformation. Generally the images of a fine grid

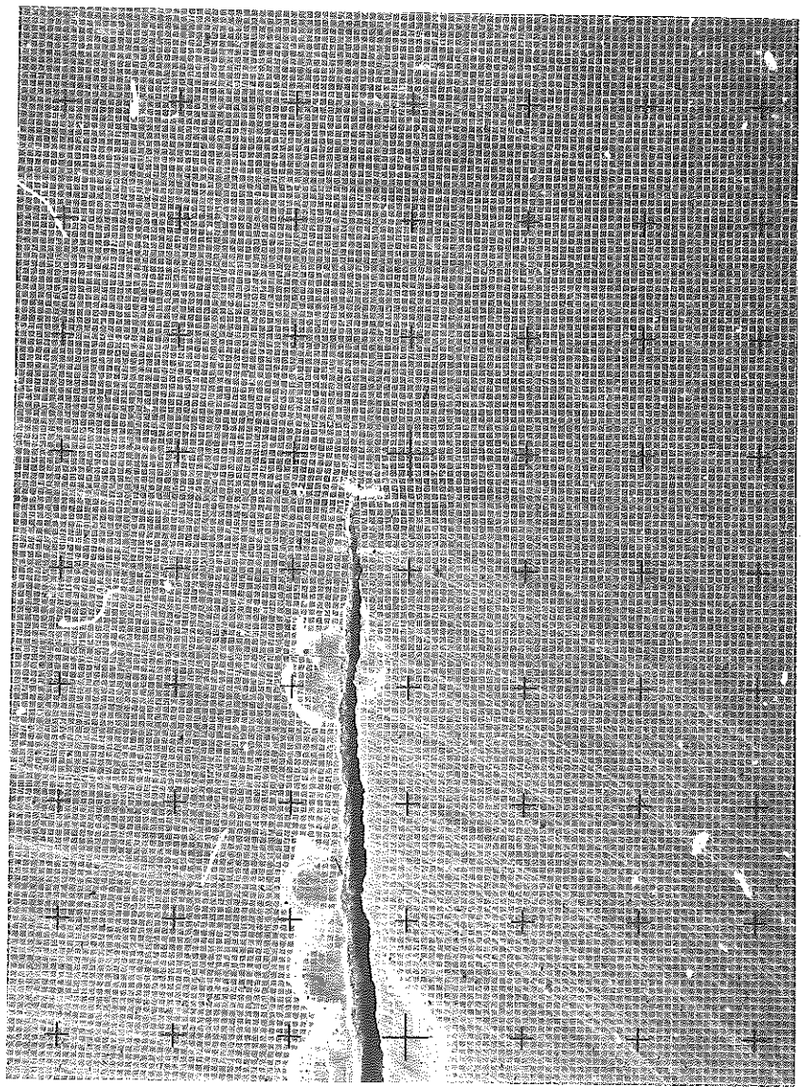

Fig 8 Grating field around the crack in the deformed state of the object with 10 lines/mm (section), including reseau marks of the recording camera

have to be taken on a film from these various stages, since a film (5 by 5 cm) resolves at least 500–1000 lines, while a CCD camera delivers 50–100 lines.

The film, in consequence, must be digitised in e.g. 10–10 segments with a conventional CCD camera to obtain the inherent resolution. The segmentation is performed using cross marks supplied by a Rollei–Reseau camera, as

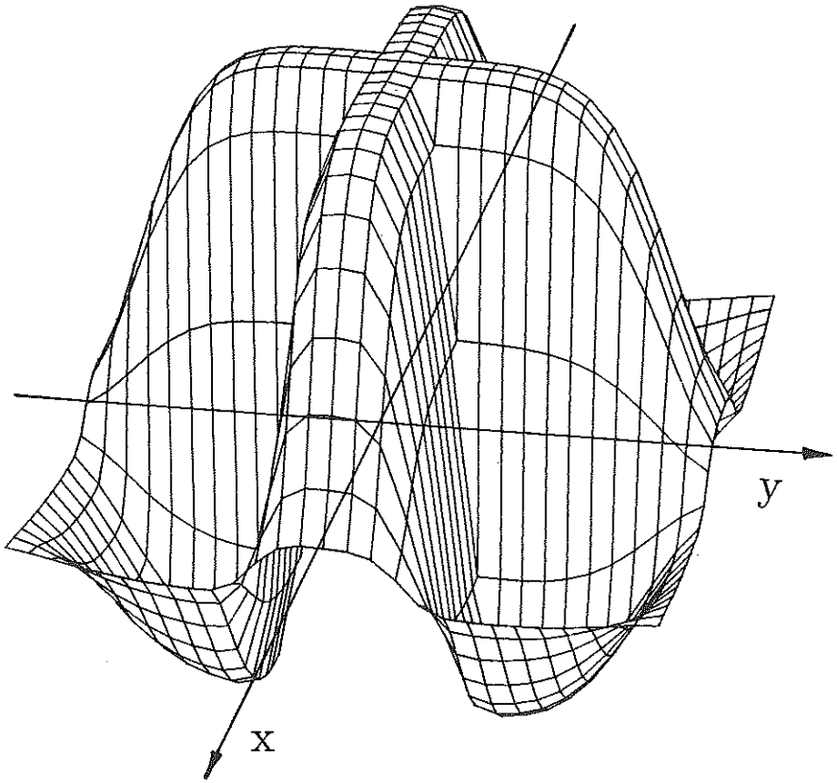

Fig 9 Correlation filter for evaluation of cross-grating coordinates

shown in Fig. 8. These marks are taken onto film with an absolute precision of about 0.5 μm together with the deformed grid. The marks are needed to connect the segments over the whole area but, moreover, they are used to correct a possible film deformation due to the developing process.

Grating coordinates

When using the grating methods, the main problem of image processing is to determine the coordinates with a sufficiently high accuracy, which means at least a standard deviation in the range of about 1/10 of a pixel. This is achieved by application of a correlation filter (Fig. 9) to the original intensity distribution of the cross-grating (Fig. 10a), yielding a related correlation function (Fig. 10b). It is smooth and convex in the neighbourhood of all points where the grating lines are crossing each other. There it can be approximated by a polynomial of second order in a 3 by 3 pixel area containing the maximum correlation value as the central point **(8)**. The maximum of this

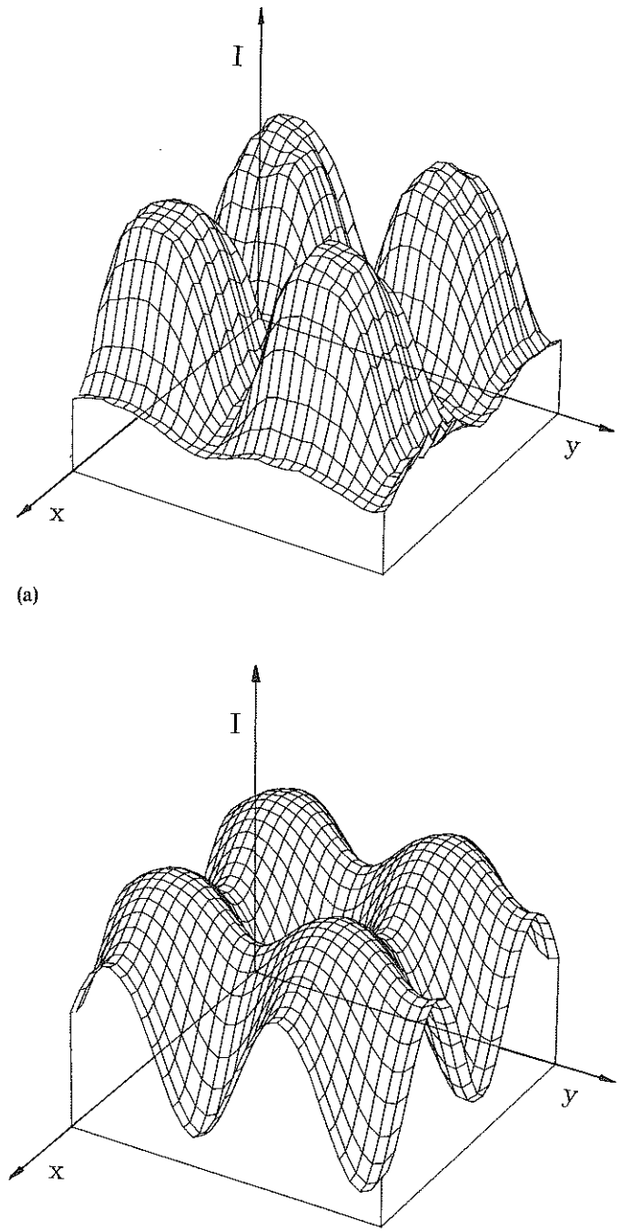

Fig 10 Cross-grating, (a) raw data, (b) interpolated and smoothened data

function then defines the grating coordinates with an accuracy of about $\pm 1/10$ pixel, provided the digitising system causes no additional error.

In order to prevent different sources of error, the whole image evaluation proceeds in the following steps, described later on in detail.

(1) Digitising a high precision quadratic reference grid and evaluating its coordinates.
(2) Calculation of a related displacement vector correcting the grid distortion caused by the digitising system.
(3) Calculation and correction of the grating coordinates in different deformation states.
(4) Smoothing and interpolation of missing coordinates.
(5) Calculation of displacement fields with respect to the undeformed state.
(6) Calculating the plane strain field using a large deformation theory and smoothing.

When digitising a film with a CCD camera, the faults of the lenses and the non-parallel planes between the film and the CCD array deform the geometry of the digitised image. Using a high precision reference grating with quadratic meshes, a correcting function can be determined reducing the failures from 1 pixel in the worst case to less than 1/10 pixel.

The coordinates of the deformed grid are determined automatically in a given area. The related program needs several initial parameters, namely the pitch of the grating, the thickness and direction of the lines, an index of a starting point, etc., which have to be submitted interactively at the beginning of the evaluation. The program then generates a consistent correlation filter and it determines about 10–20 points per second on a Microvax II computer.

These raw data are analysed with a smoothing procedure which detects gross errors, and which interpolates missing points. It smooths the grating lines in both directions separately, using first to third order two-dimensional polynomials. This procedure has to be performed in segments if the surface contains non-steady elements like cracks or holes, because averaging across these elements results in large errors for the strain.

Strain tensor for large deformations

In order to obtain the strain tensor in a point P_0 of the deformed state, the distortion of two basic vectors dr_1^0, dr_2^0 (Fig. 11) from the reference state to the deformed state dr_1^1, dr_2^1 is investigated. A plane deformation tensor can be determined from the linear relations

$$d\boldsymbol{r}_1^1 = \boldsymbol{F}\, d\boldsymbol{r}_1^0, \qquad d\boldsymbol{r}_2^1 = \boldsymbol{F}\, d\boldsymbol{r}_2^0 \tag{7}$$

This tensor $\boldsymbol{F}$, consisting of a rigid body rotation and the deformation, is split into a rotational tensor $\boldsymbol{R}$ and a large strain tensor $\boldsymbol{U}$

$$\boldsymbol{F} = \boldsymbol{R}\boldsymbol{U} \tag{8}$$

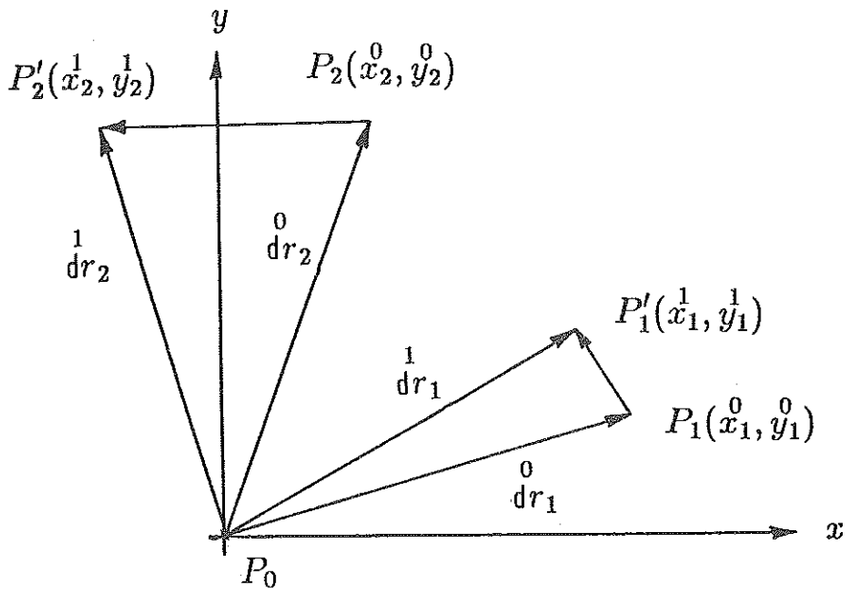

Fig 11 Basic vectors of the undeformed and the deformed state

Using the relations

$$\boldsymbol{C} = \boldsymbol{F}^{\mathrm{T}}\boldsymbol{F} = \boldsymbol{U}^{\mathrm{T}}\boldsymbol{R}^{\mathrm{T}}\boldsymbol{R}\boldsymbol{U} = \boldsymbol{U}^{\mathrm{T}}\boldsymbol{U} \tag{9}$$

it is possible to calculate, (9)

$$U = \sqrt{\boldsymbol{C}} = f_0^1 + f_1\boldsymbol{C} \tag{10}$$

where

$$f_1 = \frac{1}{\sqrt{\{\mathrm{tr}\ \boldsymbol{C} + 2\sqrt{(\det \boldsymbol{C})}\}}}; \qquad f_0 = f_1\sqrt{(\det \boldsymbol{C})} \tag{11}$$

The elements of the U tensor

$$\begin{pmatrix} U_{11} & U_{12} \\ U_{21} & U_{22} \end{pmatrix} = \begin{pmatrix} 1+\varepsilon_x & \varepsilon_{xy} \\ \varepsilon_{xy} & 1+\varepsilon_y \end{pmatrix} \tag{12}$$

correspond to the large strain components of the deformed base vectors.

This procedure is performed for each point of the grid, averaging the strain components over the deformation of the four corresponding basic vectors (10).

As a result three matrices are derived, containing the raw values ε_x, ε_y, and ε_{xy} of the strain tensor. These values can be smoothened further over 2×2 or 3×3 meshes when plotting isolines, if too much noise is present. This, however, reduces the resolution of the strain field.

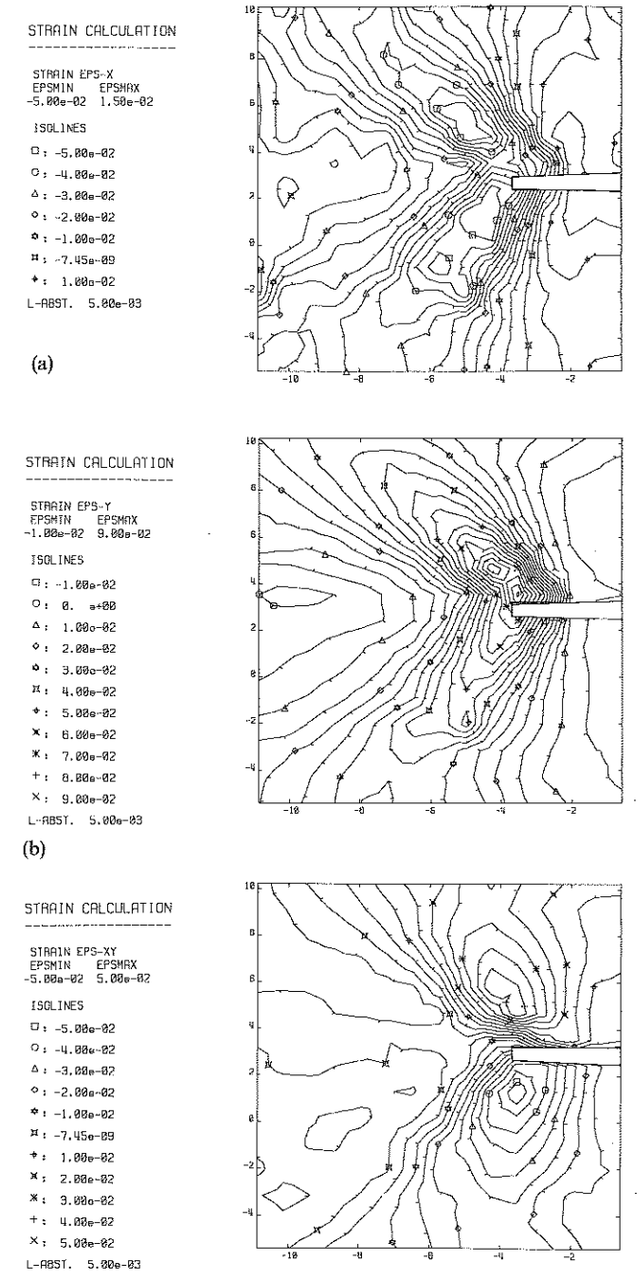

Fig 12 Strain components near the crack tip (measured) (a) ε_x, (b) ε_y, (c) ε_{xy}

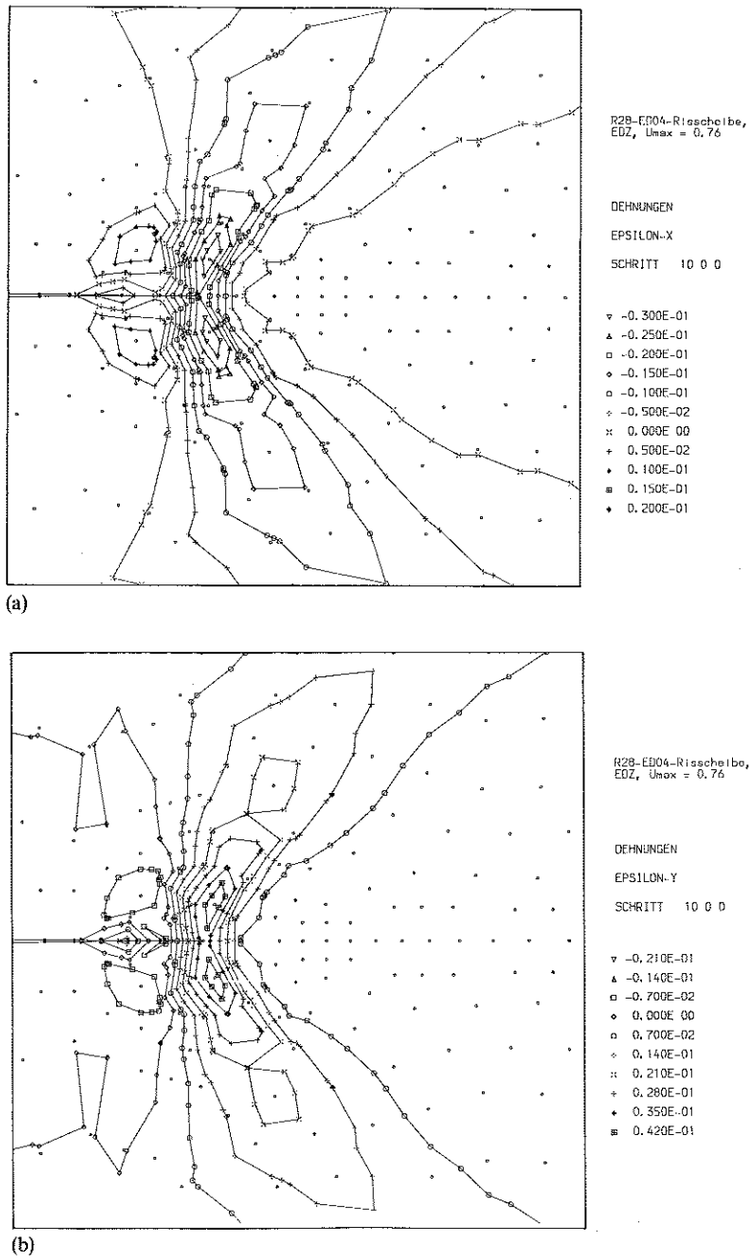

Fig 13 Strain components near the crack tip (calculated) (a) ε_x, (b) ε_y, (c) ε_{xy}

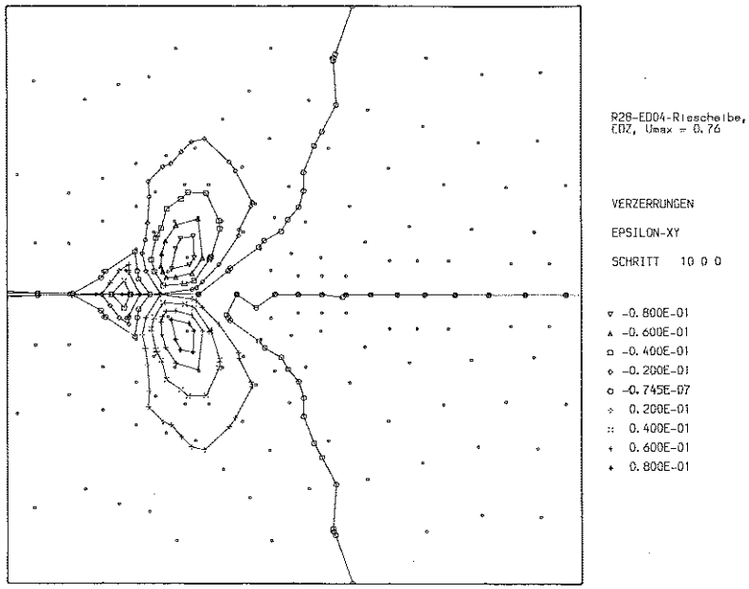

(c)

Fig 13 (continued)

By experience, the accuracy is about ± 1–3 percent strain, depending on the quality of the images. Thus the method is not suited for elastic deformations but it is a reasonable choice if strains in the range from some permille up to very large deformations of e.g. some 100 percent are to be investigated. Moreover it submits simultaneously the three plane–strain components, which is not generally possible when using Moiré- and interferometric methods.

The described grating method, including image evaluation, was applied to crack propagation in the specimen presented in section 2, loaded in bending. The strains near the crack tip are shown in Figs 12a, b, and c. Figures 13a, b, and c show the strain values calculated by the finite element program for plane strain. They agree very well with the results from experiment.

Acknowledgement

This project has been supported by the Deutsche Forschungsgemeinschaft (DFG) under contract Ste 258/4.

References

(1) ANDERSSON, H. (1973) A finite element representation of stable crack growth, *J. Mech. Phys. of Solids*, **27**, 337.
(2) DU, S. and LEE, J. D. (1983) Variations of various fracture parameters during the process of subcritical crack growth, *Engng Fracture Mech.*, **17**, 173.

(3) WESTENDORF, H. (1988) *Numerische Simulation stabilen Rißwachstums in inhomogenen elastisch–plastischen Materialien*, DVS Verlag, Düsseldorf.
(4) GRIFFITH, A. A. (1920) The phenomena of rupture and flow in solids, *Philosophical Transactions*, Royal Society of London, **A 221**, 163.
(5) ROHRBACH, Ch. (1989) *Handbuch für experimentelle Spannungsanalyse*, VDI Verlag, Düsseldorf, 279–299.
(6) CORNELIUS, V., HILBIG, J., RITTER, R., WILKE, W., and FORNO, C. L. (1989) *Zur Formanalyse mit Hilfe hochtemperaturbeständiger Raster*, VDI Ber. **731**, VDI Verlag, Düsseldorf, 295–302.
(7) ANDRESEN, K., KAMP, B., and RITTER, R. (1988) *Verformungsmessungen an Rißspitzen nach dem Objekt-Rasterverfahren*, VDI Ber. **679**, VDI Verlag, Düsseldorf, 393–403.
(8) ANDRESEN, K. and MORCHE, B. (1988) Die Ermittlung von Rasterkoordinaten und deren Genauigkeit, *Mustererkennung*, **10**, DAGM Symposium Zürich, Berlin, New York, Tokyo, 277–283.
(9) STICKFORTH, J. (1987) The square root of a three-dimensional positive tensor, *Acta Mechanica*, **67**, 233–235.
(10) ANDRESEN, K. and HORSTMANN, H. (1989) Ermittlung der Verformungen in einer gelochten Gummimembran mit Hilfe von Rasterverfahren, Forsch, Ing. Wes. **55**, 33–36.